IL NUOVO CIMENTO Vol. 33 C, N. 5 Settembre-Ottobre 2010
DOI 10.1393/ncc/i2011-10713-5

Colloquia: LaThuile10

Early physics with ALICE

F. Prino for the ALICE Collaboration
INFN, Sezione di Torino - Torino, Italy

(ricevuto il 14 Settembre 2010; pubblicato online l'11 Gennaio 2011)

Summary. — The ALICE experiment at the CERN Large Hadron Collider started its p-p data taking at the end of 2009. The availability of the first low luminosity collisions at $\sqrt{s} = 900\,\text{GeV}$ and $\sqrt{s} = 2.36\,\text{TeV}$ allowed to improve and extend the calibration and alignment procedures, started with cosmic rays in 2008. Together with the final commissioning of the detector with real data, the collected data sample of p-p collisions is presently being used to carry out the early physics studies, aimed at assessing the global characteristics of the interaction. In particular, results on the pseudorapidity density of primary charged particle in the central region are discussed here. They were obtained using the two innermost Silicon Pixel layers of the Inner Tracking System, which provided both the primary vertex position and the charged multiplicity, by matching the reconstructed points on the two layers.

PACS 13.85.-t – Hadron-induced high- and super-high-energy interactions.
PACS 29.40.Gx – Tracking and position-sensitive detectors.

1. – The ALICE experiment

ALICE [1] is a general-purpose detector for the study of p-p, p-A and heavy-ion collisions at the LHC [2]. The main physics goal of the experiment is to investigate the properties of strongly-interacting matter in the conditions of high temperature and energy density that are expected to be attained in Pb-Pb collisions at $\sqrt{s_{\text{NN}}} = 5.5\,\text{TeV}$.

The main components of the ALICE detector are a central tracking and particle identification system, a forward muon spectrometer and a set of small detectors in the forward regions used for triggering and global event characterization purposes. The central barrel detectors cover the pseudorapidity range $-0.9 < \eta < 0.9$ and are embedded in the large L3 solenoidal magnet which provides a field of 0.5 T. The main tracking detector in the central rapidity region is a large Time Projection Chamber (TPC) with inner radius of about 85 cm and outer radius of about 250 cm and an overall length along the beam direction of 500 cm. Inside the TPC, a barrel-type silicon tracker called Inner Tracking System is mounted. Outside the TPC, three detectors dedicated to particle identification, namely a Transition Radiation Detector (TRD), a Time-of-Flight detector

(TOF) and a ring-imaging Cherenkov detector (HMPID) are installed together with two electromagnetic calorimeters (PHOS and EMCal).

The Inner Tracking System (ITS) is the central barrel detector located closest to the beam axis and is composed of six cylindrical layers of silicon detectors with radii between 3.9 cm and 43.0 cm. The two innermost layers are equipped with Silicon Pixel Detectors (SPD), the two intermediate layers are made of Silicon Drift Detectors (SDD), while Silicon Strip Detectors (SSD) are mounted on the two outermost layers. The main task of the ITS is to provide precise track and vertex reconstruction close to the interaction point, improving the spatial, angular and momentum resolution for tracks reconstructed in the TPC. Moreover, it allows to recover particles that are missed by the TPC (due to either dead regions or low-momentum cut-off), to reconstruct the interaction vertex with a resolution better than 100 μm and to identify the secondary vertices from the decay of hyperons and heavy flavoured hadrons [2]. In addition to that, the track segments (tracklets) built in the two pixel layers provide the initial estimate of the interaction vertex position, prior to full track reconstruction, and a measurement of the charged particle multiplicity in the pseudorapidity range covered by the SPD layers.

Among the forward detectors, the VZERO has an important role in the early physics analyses described here. It consists of two arrays of 32 scintillators each, which are placed around the beam pipe on either side of the interaction region. The two arrays cover the pseudorapidity ranges $2.8 < \eta < 5.1$ and $-3.7 < \eta < -1.7$, respectively. They record the arrival times of particles at the detector in a time window of ± 25 ns around the nominal beam crossing time.

2. – Detector commissioning

All the installed ALICE detectors have been extensively commissioned, calibrated and used for data taking during the two long cosmic ray runs collected in summer 2008 and summer 2009 [3-6]. A large number of sub-detector specific calibration runs have also been collected in these periods to monitor the stability of the detector performance during various months of continuous operation. Data were also taken during various LHC injection tests to perform timing measurements and other calibrations.

2˙1. *ITS*. – The cosmic rays triggered by the SPD allowed to obtain an initial alignment of the parts of the detector that had sufficient exposure to the mostly vertical cosmic ray flux [7]. This has been obtained by applying track-based alignment methods (namely the Millepede II [8] and an iterative local method) starting from the information of the geometrical survey measurements performed (for SDD and SSD) during the construction phase.

In particular, the SPD layers of the ITS, which are the main detectors used for multiplicity measurement, were aligned using cosmic-ray tracks [7]; the residual misalignment was estimated to be below 10 μm for the modules well covered by mostly vertical tracks. This estimate has been extracted from different observables sensitive to the alignment quality. As an example, in fig. 1 (left) the distance in the bending plane between points attached to the same track in the region where there is an acceptance overlap between two modules of the same layer is displayed, before and after the Millepede alignment. The spread of the distribution after re-alignment is $\sigma \approx 18\,\mu$m, to be compared to $\sigma \approx 15\,\mu$m obtained in simulations with ideal geometry.

For SSD, the geometrical survey already provided a very precise alignment, as can be seen in fig. 1 (right) which shows the distribution of the $r\varphi$ residuals between tracks

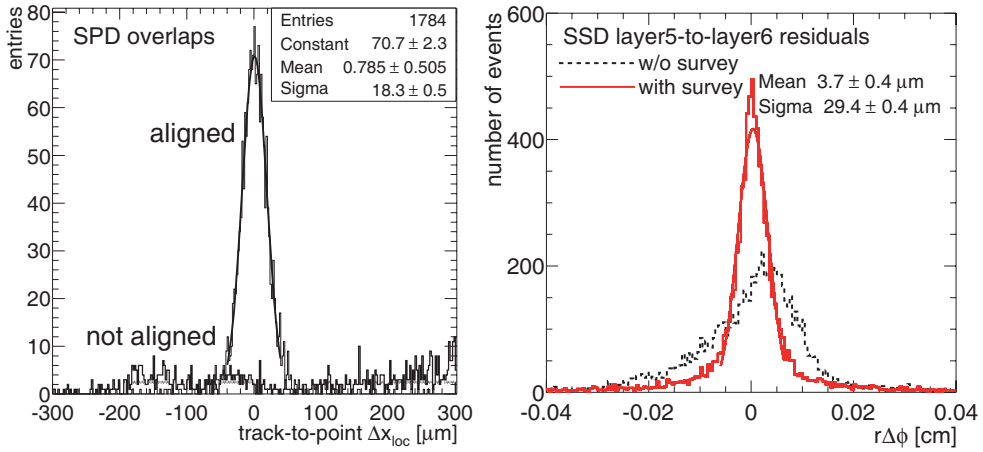

Fig. 1. – Left: track-to-point residuals in the bending plane for SPD double points in acceptance overlaps before and after alignment. Right: distribution of the $r\varphi$ residuals between straight-line tracks defined from two points on SSD layer 6 and the corresponding points on SSD layer 5, with and without applying geometrical information from the survey.

through layer 6 (built from the two points in the top and bottom halves of the barrel) and points on layer 5, before and after applying the geometrical information extracted from the survey. This analysis allowed to estimate the residual misalignment after the survey to be at the level of 5–20 μm (for modules and assemblies of modules, respectively). For this reason, track-based alignment methods were used only to align the whole SPD barrel with respect to the SSD barrel and to optimize the positioning of large sets of SSD modules, namely the upper and lower halves of layers 5 and 6. On top of this, cosmic-ray data was used for SSD gain calibration, allowing in particular to refine the relative calibration of the P and N sides. This charge matching is a strong point of double-sided silicon sensors and helps to remove fake clusters.

The alignment of the SDD is challenged by the interplay with time zero (*i.e.* the measured drift time for particles with zero drift distance) and drift speed calibration. During the cosmic run, it was possible to have a frequent monitoring of the drift speed in many different positions on each of the 260 detector modules, using the MOS charge injectors integrated on the detector surface [5]. This allowed to tune the drift speed calibration procedure and to study the drift speed stability on a long time scale. The cosmic ray tracks allowed to develop the methods to extract the time-zero and the drift speed (for modules with mal-functioning injectors) from track-to-point residuals. However, cosmics tracks are not the ideal sample for this purpose because of the jitter between the time when the muon crosses the detectors and the trigger signal. Hence, the SDD alignment is currently being extracted from p-p data. Cosmic rays were also used to tune the absolute calibration of the $\mathrm{d}E/\mathrm{d}x$ signal and to test the linear correction for the dependence of the reconstructed charge on the drift time due to the combined effect of charge diffusion and zero suppression [9].

2˙2. *TPC.* – Calibration and commissioning of the ALICE TPC relied, before the availability of any collisions from the LHC, on three different methods: a set of UV

laser beams was used to characterize field distortions and to determine the magnitude of the correction from $E \times B$ effects on the drifting electrons originating from the residual non-parallelism of the electric and magnetic field inside the drift volume. Furthermore, radioactive krypton was inserted through the gas system into the detector to provide efficient and precise amplitude calibration of all 557568 readout channels. Finally, extensive measurements with cosmic rays were performed to determine tracking efficiencies, energy loss, and momentum resolution of the detector. Detailed results can be found in [6].

3. – Early physics analyses

The primary goal of the early physics analyses performed on p-p data collected by the ALICE experiment in the new energy regime attained at the LHC is the measurement of the global characteristics of the collisions, which are dominated by soft (*i.e.* small-momentum-transfer) processes. These observables are useful to study QCD in the non-perturbative regime, to constrain phenomenological models and event generators and to understand the backgrounds for measurements of hard and rare interactions.

3˙1. *Charged-particle pseudorapidity density.* – The pseudorapidity density of charged primary particles has been estimated from the "tracklets" reconstructed by correlating hits in the two silicon-pixel layers. A first analysis has been performed on the very first sample of 284 proton-proton collisions collected on 23rd November 2009, at a centre-of-mass energy $\sqrt{s} = 900\,\text{GeV}$, during the commissioning of the accelerator [10]. The analysis has then been repeated on larger statistics and with improved trigger selection on a sample of about 150000 interactions at 900 GeV as well as on about 40000 collisions at 2.36 TeV [11].

The event sample was collected with the ALICE Minimum-Bias (MB) trigger based on SPD and VZERO information. At 900 GeV, the MB trigger required a hit in either one of the VZERO counters or in the SPD detector; *i.e.* essentially at least one charged particle anywhere in the 8 units of pseudorapidity covered by these trigger detectors. At the higher energy, the trigger required at least one hit in the SPD detector ($|\eta| < 2$), since the VZERO was not available. The events were collected in coincidence with the signals from two beam pick-up counters (BPTX), one on each side of the interaction region, indicating the presence of passing bunches.

Events which pass some background rejection criteria and which have a reconstructed interaction vertex are selected for the analysis. The pile-up probability is negligible at the typical bunch intensities (5×10^9 protons) of the data-taking period considered here. Beam-gas and beam-halo background events were removed by a cut on the ratio between the number of tracklets and the total number of hits in the ITS. For the 900 GeV data, also VZERO counters were used for background rejection by requiring their timing signals to be compatible with particles produced in collision events. In addition, for 900 GeV data, MB events in coincidence with only one passing bunch, as well as when no bunch was passing through the detector, were also registered. These control triggers were used to measure the beam-induced and accidental backgrounds. The position of the interaction vertex is reconstructed [12] by correlating hits in the two SPD layers. The achieved resolution depends on the track multiplicity and is approximately 100–300 μm in the longitudinal direction and 200–500 μm in the transverse direction. For events with only one charged track, the vertex position is determined by intersecting the SPD tracklet with the mean beam axis determined from the vertex positions of other events in the sample. A vertex was reconstructed in 94% of the selected events. The vertex reconstruction

efficiency decreases for collisions occurring far from the centre of the detector (*i.e.* large $|z|$ values), due to the reduced acceptance of the SPD detector for largely displaced interaction vertices. Therefore, only events with vertices within $|z| < 10\,\text{cm}$ were used. This allows for an accurate charged-particle density measurement in the pseudorapidity range $|\eta| < 1.6$ using both SPD layers.

The number of primary charged particles is estimated by counting the number of tracklets built by matching pairs of hits in the two SPD layers using the reconstructed vertex as the origin. The matching is based on a selection on the sum of the squares of the differences in azimuthal ($\Delta\varphi$, bending plane) and polar ($\Delta\theta$, non-bending direction) angles [13]. When more than one hit in a layer matches a hit in the other layer, only the hit combination with the smallest angular difference is used. This occurs in only 2% of the matched hits. The measured number of tracklets is corrected for geometrical acceptance, detector and reconstruction inefficiencies, combinatorial background caused by an accidental association of hits in the two SPD layers, contamination by decay products of long-lived particles (K^0_s, Λ, etc.), gamma conversions and secondary interactions.

The total number of collisions used for the normalization was calculated from the number of events selected for the analysis which contains three different classes of inelastic interactions, *i.e.* collisions where new particles are produced: non-diffractive (ND), single-diffractive (SD), and double-diffractive (DD). Experimentally we cannot distinguish among these classes, which, however, are selected by the MB trigger with different efficiencies. In order to compare our data with those of other experiments, the resulting multiplicities are given with two different normalizations: the first one (INEL) corresponds to the sum of all inelastic interactions, and corrects the trigger bias individually for all event classes, by weighting them, each with its own estimated trigger efficiency and abundance. The second normalization (non-single-diffractive or NSD) applies this correction for non-diffractive and double-diffractive processes only, while removing, on average, the single-diffractive contribution. The normalization for INEL and NSD events was obtained by correcting the number of selected events for the trigger and the vertex-reconstruction efficiencies.

For the first analysis on the very first data sample, these efficiencies have been extracted from Monte Carlo simulations separately for ND, SD and DD processes and weighted with their measured cross-sections. In addition, for NSD events, the single-diffractive contribution has been subtracted. The resulting charged-particle density as a function of pseudorapidity is shown in fig. 2 (left) together $p\bar{p}$ data from the UA5 experiment [14].

In the analysis performed successively on larger statistics, two different event samples were used for the measurement of INEL and NSD multiplicities at 900 GeV. For the INEL analysis, events fulfilling a trigger condition requiring logical OR between the signals from the SPD and VZERO detectors were used. For the NSD analysis, a subset of the total sample was selected by requiring a coincidence between the two sides of the VZERO detectors (*i.e.* the detection of at least one charged particle in both the forward and backward hemispheres, separated by 4.5 units of pseudorapidity). In this subset, single-diffraction events are suppressed, therefore, model-dependent corrections and associated systematic errors are reduced. With these selections, the resulting total systematic uncertainty on the pseudorapidity density measurement at 900 GeV is smaller than 2.5% for INEL collisions and is about 3.3% for NSD collisions [11]. The resulting charged-particle density as a function of pseudorapidity obtained for INEL and NSD interactions at a centre-of-mass energy $\sqrt{s} = 900\,\text{GeV}$ compared to $p\bar{p}$ data from the UA5 experiment [14], and to pp NSD data from the CMS experiment [15] is shown in fig. 2 (right).

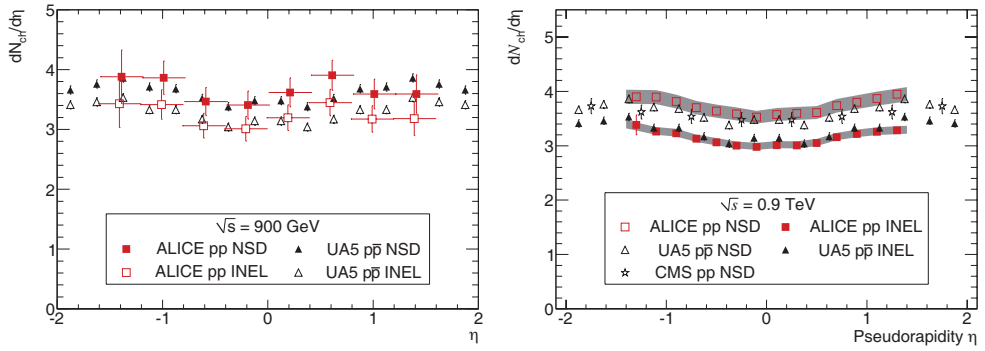

Fig. 2. – Measured $\mathrm{d}N_{\mathrm{ch}}/\mathrm{d}\eta$ of at $\sqrt{s} = 900\,\mathrm{GeV}$ for INEL and NSD collisions from the very first data samples of 284 p-p collisions (left) and from a larger data sample (right).

The same analysis has been repeated on the sample of collisions collected at $\sqrt{s} = 2.36\,\mathrm{TeV}$. Figure 3 shows the centre-of-mass energy dependence of the pseudorapidity density in the central region. The measured charged particle density at the higher energy is consistent with the CMS result for NSD collisions. The observed relative increase in multiplicity between the two energies ($22.6 \pm 0.7 \pm 1.0\%$) results to be substantially larger than the one predicted by PYTHIA (tested with three different tunes) and PHOJET models [11].

3˙2. *Other ongoing analyses.* – The statistics collected from the first data sample of proton-proton collisions at the LHC is presently being used in many other analyses aimed at studying the global characteristics of collisions at $\sqrt{s} = 900\,\mathrm{GeV}$. Multiplicity distributions have been measured [11]. The proton–to–anti-proton ratio has been measured with high precision and found to be very close to unity, as expected in the standard picture of baryon transport at this energy. In addition, p_T spectra of charge hadrons have been reconstructed up to $10\,\mathrm{GeV}/c$ and compared with previous Sp$\bar{\mathrm{p}}$S measurements and

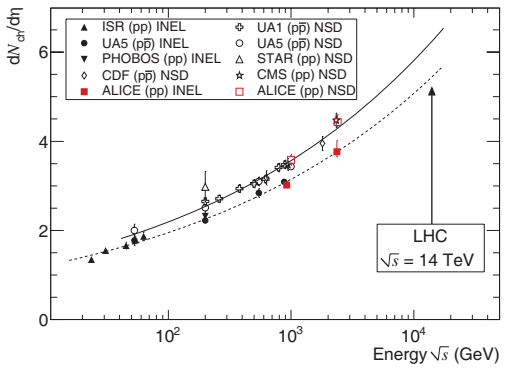

Fig. 3. – Charged-particle pseudorapidity density in the central rapidity region in proton-proton and proton-antiproton interactions as a function of the centre-of-mass energy. The dashed and solid lines (for INEL and NSD interactions, respectively) show a fit with a power-law dependence on energy.

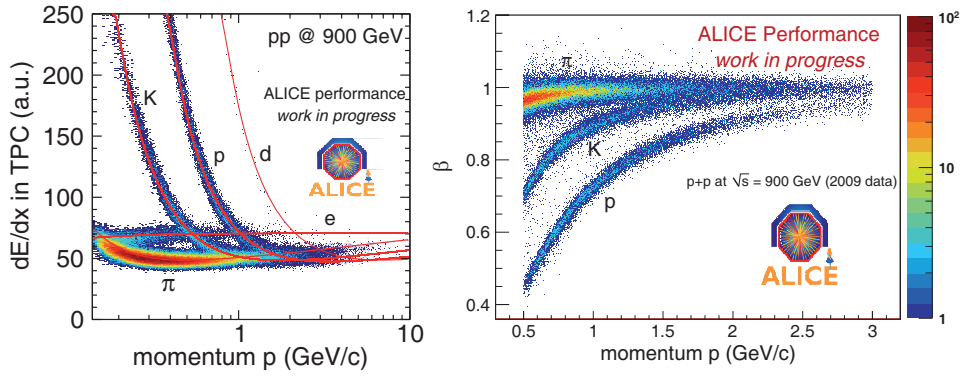

Fig. 4. – Particle identification performance in p-p 2009 data sample. Left: measured energy-deposit of charged particles *vs.* their momentum in the TPC. The lines correspond to the ALEPH parameterization of the Bethe-Bloch curve. Right: dependence of the particle velocity measured by TOF on the particle momentum.

also with CMS results [15]. This allows also to study the increase of average p_T as a function of event multiplicity. Transverse momentum spectra are being reconstructed also for identified hadrons (π, K and p) in an extended p_T range by exploiting the particle identification capabilities provided by the $\mathrm{d}E/\mathrm{d}x$ measurement in the TPC, the TOF information for high-momentum particles and by the ITS stand-alone tracks in the low-p_T region (*i.e.* below 200 MeV/c). The particle identification performance is illustrated in fig. 4 for the TPC (measured $\mathrm{d}E/\mathrm{d}x$ as a function of momentum) and TOF (measured particle velocity as a function of momentum) detectors. Strangeness production is also being measured from topological reconstruction of K^0_s, Λ and Ξ decays.

4. – Conclusions

The first samples of proton-proton collisions at the LHC at $\sqrt{s} = 900\,\mathrm{GeV}$ and 2.36 TeV allowed to perform high-precision measurements of the global characteristics of the collision with the ALICE detector. In particular, the pseudorapidity density of charged primary particles showed a larger-than-expected enhancement of multiplicity when increasing the center-of-mass energy from $\sqrt{s} = 900\,\mathrm{GeV}$ to 2.36 TeV.

REFERENCES

[1] ALICE Collaboration, *JINST*, **3** (2008) S08002.
[2] ALICE Collaboration, *J. Phys. G: Nucl. Part. Phys.*, **32** (2006) 1295.
[3] Kuijer P. G. for the ALICE Collaboration, *Nucl. Phys. A*, **830** (2009) 81C.
[4] Santoro R. *et al.*, *JINST*, **4** (2009) P03023.
[5] Alessandro B. *et al.*, *JINST*, **5** (2010) P04004.
[6] Alme J. *et al.*, arXiv:1001.1950 (2010).
[7] ALICE Collaboration, *JINST*, **5** (2010) P03003.
[8] Blobel V., *Nucl. Instrum. Methods A*, **566** (2006) 5.
[9] Alessandro B. *et al.*, *JINST*, **5** (2010) P02008.

[10] Aamodt K. *et al.* (ALICE Collaboration), *Eur. Phys. J. C*, **65** (2010) 111.
[11] Aamodt K. *et al.* (ALICE Collaboration), arXiv:1004.3034 (2010).
[12] Bruna E. *et al.*, ALICE Internal Note ALICE-INT-2009-018 (2009).
[13] Elia D. *et al.*, ALICE Internal Note ALICE-INT-2009-021 (2009).
[14] Alner G. J. *et al.* (UA5 Collaboration), *Z. Phys. C*, **33** (1986) 1.
[15] CMS Collaboration, *JHEP*, **02** (2010) 041.